Oxygen adsorbates on the Si(111)4×1-In metallic atomic wire: Scanning tunneling microscopy and density-functional theory calculations

Deok Mahn Oh,[1,2] S. Wippermann,[3] W. G. Schmidt,[4] and Han Woong Yeom[1,2,*]

[1]*Center for Artificial Low Dimensional Electronic Systems, Institute for Basic Science (IBS), Pohang 790-784, Korea*

[2]*Department of Physics, Pohang University of Science and Technology, Pohang 790-784, Korea*

[3]*Interface Chemistry and Surface Engineering Department, Max-Planck-Institute for Iron Research GmbH, Max-Planck-Straβe 1, 40237 Düsseldorf, Germany*

[4]*Lehrstuhl für Theoretische Physik, Universität Paderborn, 33098 Paderborn, Germany*

(Received 23 May 2014; revised manuscript received 23 August 2014; published 20 October 2014)

The Si(111)4×1-In surface is composed of metallic atomic wires, which undergo a transition into a charge density wave phase at a transition temperature (T_c) of 125 K. This T_c was reported recently to substantially increase upon the oxygen adsorption, for which the underlying mechanism is not understood. We investigate the structures of oxygen adsorbates on the Si(111)4×1-In surface by scanning tunneling microscopy (STM) and density-functional theory calculations. We identify three distinct atomic-scale structures induced by the oxygen adsorption with high-resolution STM topography. The calculations find two energetically favorable adsorption sites on and between In zigzag chains, respectively. In conjunction with an additional adsorption configuration, where O is buried underneath the In chain, three stable structures are thus identified that reproduce very well the characteristic bias-dependent STM images. Experimentally, a switching between two specific adsorption structures is observed and is consistent with the structure models proposed. The structural distortions and the charge transfer of In atomic wires around the adsorbates are also characterized. This work provides a solid basis for the microscopic understanding of the intriguing oxygen impurity effect on the phase transition.

DOI: 10.1103/PhysRevB.90.155432 PACS number(s): 68.65.−k, 68.47.De, 68.43.Fg, 68.37.Ef

I. INTRODUCTION

Atomic and nanoscale one-dimensional (1D) materials are interesting not only because of their potential applications in future nanometer- or atomic-size devices [1,2] but also because of exotic properties that emerge due to enhanced many-body interactions [3,4]. Within such 1D materials, the presence of a very small density of defects or impurities can drastically modify physical properties, providing both a challenging barrier to understand their physics and the exciting opportunity to control them [5,6]. In particular, there are diverse impurity effects discussed in 1D charge density wave (CDW) [7] materials such as the pinning of the CDW fluctuations [8,9] and the suppression or enhancement of the CDW order [10]. While there have been various theoretical and experimental studies, there are few atomic-scale experimental investigations for the 1D CDW-impurity interaction. The previous scanning tunneling microscopy (STM) studies for the CDW-impurity interaction mostly dealt with 2D CDW systems [11–14] and impurities therein were often not so well characterized.

In this respect, the oxygen impurity on the Si(111)4×1-In (hereafter 4×1-In) surface deserves particular attention. The 4×1-In surface consists of indium atomic wires self-organized into a well-ordered array and exhibits a metal-insulator transition at a transition temperature (T_c) of 125 K into the periodicity-doubled CDW phase called 8×2-In [4,15]. The interactions of the impurities on this system have been extensively studied [16–20] and the role of impurities in the phase transition is under debate currently [21–23]. In stark contrast to the fact that most of adsorbate impurities on this surface were shown to suppress the CDW order locally and globally [16–19], the oxygen adsorption was intriguingly reported to increase T_c substantially [17,19]. The angle-resolved photoelectron spectroscopy (ARPES) study subsequently confirmed that this apparent phase change above the pristine T_c is indeed due to the metal-insulator phase transition [24]. While the suppression of the CDW long-range order might easily be understood from the trivial random impurity effect [25–27] or the doping effect [20], the enhanced T_c seems to indicate a novel impurity-CDW interaction. Initially, two different mechanisms were proposed to explain this phenomenon: (i) the nonrandom distribution of oxygen adsorbates and (ii) the hole doping by oxygen adsorbates [17]. The hole doping case was not supported by the recent ARPES study [24]. In order to investigate this issue further, it is highly required to characterize the distribution and atomic structures of oxygen adsorbates.

In the present work, we perform an extensive STM study together with density-functional theory (DFT) calculations for the oxygen adsorption on the 4×1-In surface. From the STM measurements, we identify three distinct structures induced by the oxygen adsorption. The adsorbate-induced structures are randomly distributed and their diffusion is not active at room temperature. Bias-dependent STM images of these structures are in excellent agreement with the simulated STM images based on the energetically favorable adsorbate structures of DFT calculations. In addition, the switching between two different adsorption structures is observed, which can be consistently explained by our structure models. We also quantify the interactions of the adsorbate and the In wire in terms of the lattice distortion and the charge transfer. The atomic structures of oxygen adsorbates and the charge-lattice distortions around them established here provide a solid basis for understanding the intriguing oxygen-CDW interaction

*To whom all correspondence should be addressed: yeom@postech.ac.kr

of the present system at low temperature, narrowing down substantially possible mechanisms of the CDW T_c increase.

II. EXPERIMENTS AND CALCULATION

The experiments were conducted using a commercial ultrahigh-vacuum STM (Omicron, Germany) at room temperature. The base pressure was kept below 2×10^{-11} Torr. An n-doped Si(111) surface was cleaned by repeated heating up to 1500 K. The 4×1-In surface was prepared by depositing one monolayer of In onto a clean Si(111)7×7 surface at 570 K [4]. Oxygen molecules were carefully dosed at room temperature by backfilling the STM chamber through a precision leak valve. The dosage was measured by a quadrupole mass spectrometer. The DFT calculations were performed within the local density approximation (LDA) [28] as implemented in the Vienna *Ab initio* Simulation Package (VASP) [29]. Indium 4d electrons were treated as core electrons. The surface was modeled using three Si bilayers. A 8×12 surface unit cell was used, apart from the adsorption energy surface calculations which were performed using a 8×8 lateral periodicity. The Brillouin zone integration was performed using a k-point sampling equivalent to 256 points within a 1×1 unit cell.

III. RESULTS AND DISCUSSION

Figures 1(a) to 1(c) show the STM images before and after oxygen exposures. The STM image of the pristine 4×1-In surface shows unit wires arrayed regularly, each of which is composed of two bright rows [Fig. 1(a)]. These rows of protrusions with the a_0 periodicity correspond to metallic In zigzag chains [15]. Before the exposure, one can observe characteristic native defects appearing as V-shaped depressions

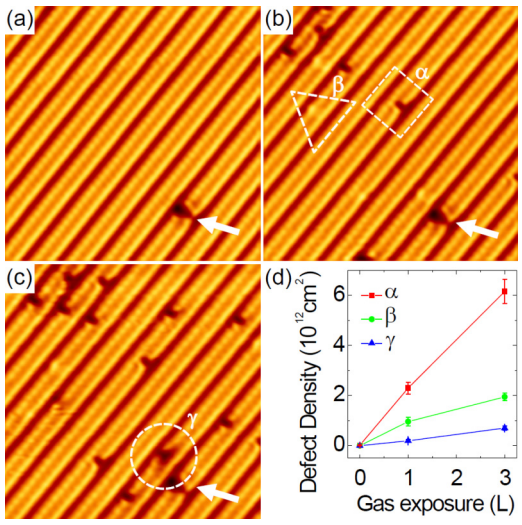

FIG. 1. (Color online) STM images of the Si(111)4×1-In surface (a) before the exposure and after exposures to oxygen dosage of (b) 1 and (c) 3 L. All STM images were taken on the same area (13 nm × 13 nm) with a tunneling bias $V_s = -1.0$ V and a tunneling current $I_t = 50$ pA. The white arrows indicate a native defect used as a position reference. (d) The number of three characterized defects, which are marked with dashed line in (b) as α and β, and in (c) as γ, with respect to the oxygen exposure.

[arrows in Figs. 1(a) to 1(c)] [30]. After the exposure, three new distinct defect structures appear [Figs. 1(b) and 1(c)]. The most popular one appears as a depression on one In zigzag chain of a wire and is labeled as α [the rectangle in Fig. 1(b)]. Weak protrusions on In zigzag chains, labeled as β [the triangle in Fig. 1(b)], are also observed. The third type, labeled as γ, exhibits a similar depression to α but spreads wider in between two In chains at this particular bias [the circle in Fig. 1(c)]. However, the bias dependence of STM images for the γ defect is clearly different from α as discussed below. These defects are found to increase in number systematically upon increasing the oxygen exposure [Fig. 1(d)]. The population ratio between three defects as counted in STM images is roughly consistent at different oxygen dosages as about $\alpha : \beta : \gamma = 10 : 3 : 1$. α defects are the most frequently and dominantly observed. The appearance of α and β defects in this bias is consistent with the previous study [17]. On the other hand, γ defects were not identified before probably since they are rare and difficult to distinguish from α defects. Note that the distribution of the defects is largely random and static indicating that the adsorbate diffusion is not active at room temperature. This rules out the possible effect of the active adsorbate rearrangement to affect the transition temperature, which was suggested in the previous study [17].

The position of the depression (protrusion) of the α (β) defect is on top of one protrusion of the In zigzag chain, as we can see in the enlarged STM images of Fig. 2. In contrast, the depression of the γ defect locates between two protrusions and in the middle of two In zigzag chains. The lateral adsorption sites of the oxygen adatom in the α and β defects appear to be the same, but different from that in the γ defect. All defects exhibit the mirror symmetry with the mirror axis perpendicular to the wire.

We obtained extensive bias-dependent STM images of oxygen-induced defects (Fig. 2). The α defect shows the most noticeable bias dependence. The strong depression in the filled-state STM images is not observed at low biases of ±0.2 V and appears again at +1.0 V. In contrast, the protrusion of the β defect does not show a substantial bias-dependence. However, one can note the similarity between the STM images of the α defect and those of β in the whole bias range except for the central depression or protrusion. The α and γ defects in the STM images acquired at −1.0 V look rather similar as mentioned above but their bias dependence is distinct. The depression in the STM images of the γ defects appears both on one In zigzag chain and between the two zigzag chains. This depression is persistent at all biases.

Through DFT calculations, we establish the atomic structure models of oxygen-induced defects. As the first step, we looked for lateral sites of an oxygen adatom by calculating the adsorption energy surface (AES). The lateral position dependent adsorption energies for a single oxygen atom per 8×8 surface unit cell are calculated [Fig. 3(a)]. The present results differ slightly from the previous AES calculations [31] which were performed in a smaller 4×3 unit cell that gives rise to noticeable adatom-adatom interactions because of the periodic boundary conditions. In the AES, two sites that correspond to energy minima (the maxima in the energy gain by the adsorption) are identified [marked by X in Fig. 3(a)]. One site (red X marked) is the intrachain site, which is located

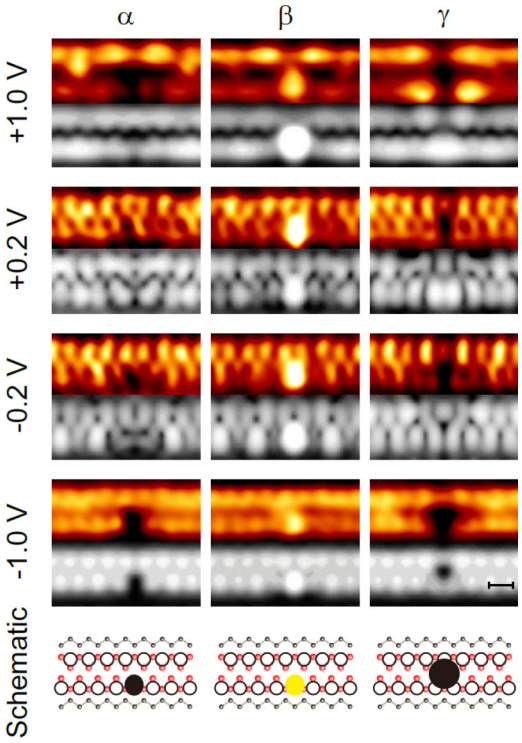

FIG. 2. (Color online) High-resolution bias-dependent STM images with simulated STM images (in gray scale) of three oxygen-induced defects at the indicated bias ($I_t = 50$ pA). The scale bar is 0.5 nm. The bottom row shows the schematics of images together with the 4×1-In structure model; red (gray) balls represent the indium (silicon) atoms and empty circles the ×1 protrusions in the STM image of 4×1-In. The depression (the protrusion) of the oxygen-induced defects is represented with the black (yellow) filled circles.

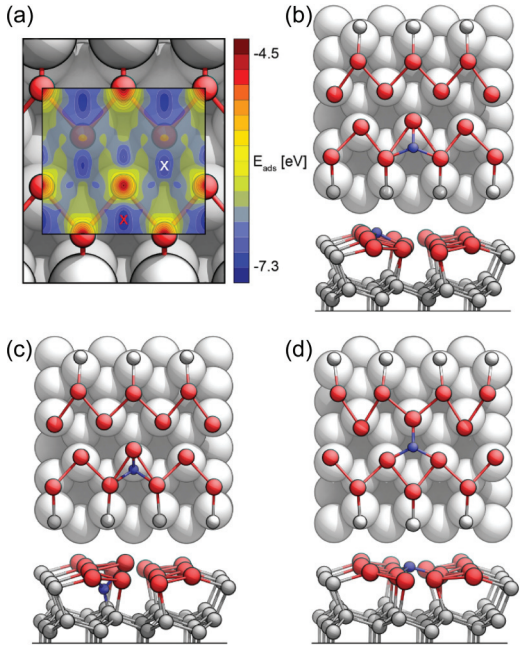

FIG. 3. (Color) (a) Adsorption energy surface (AES) calculated for an oxygen adatom on the Si(111)4×1-In surface overlaid on the 4×1-In structure model. The color scale shows the relative adsorption energy. Top and side views of the atomic models relaxed on the intrachain site [red X in (a)] [(b) and (c) for the α and β defects, respectively] and (d) on the interchain site [white X in (a)] for the γ defect. Blue, red, and white balls in the structure models are oxygen, indium, and silicon atoms, respectively.

in the center of an In trimer. The other site (white X marked) is the interchain site, located between two In zigzag chains close to one inner In atom.

Consecutively, we put an oxygen adatom on these adsorption sites and relaxed the surface structure without any constraint. Depending on the precise starting configuration, i.e., the vertical O position, the adatom in the intrachain site may assume two different stable structures. In one structure, three In-O bondings are formed within the In zigzag chain and the oxygen adatom is located slightly above In atoms [Fig. 3(b)]. The calculated adsorption energy is −7.33 eV. The simulated STM images based on this structure agree well with the experimental images of the α defect (Fig. 2). The depression of filled states and its disappearance at the low biases of ±0.2 V are excellently reproduced in the simulation. On the other hand, the oxygen adatom in this site can go underneath the In zigzag chain [Fig. 3(c)]. The number of In-O bondings is the same but, additionally, a weak Si-O bonding is formed with the Si atom in the second layer. Because of this subsurface position and the Si-O bonding, one In atom is lifted upwards. The calculated adsorption energy in this structure is −7.86 eV. This model explains well the bias-dependent STM images of the β defect. The protrusion of the β defect appears at all biases and is understood as due to the In atom lifted up. Moreover, these two relaxed structures in the same intrachain site naturally explain the similarity between the bias-dependent STM images of the α and β defects around the depression and the protrusion in their centers. The adsorption energy of the β structure is lower than α. However, the corresponding minima are separated by an energy barrier, which explains the abundance of the α defect for the room temperature adsorption.

The oxygen adatom on the interchain site is relaxed into a unique energy minimized structure [Fig. 3(d)]. On this site, the oxygen adatom forms one In-O bonding with one In zigzag chain and two In-O bondings with the other chain. The oxygen adatom is located almost at the same height as the In atoms. The comparatively small adsorption energy of 7.14 eV may explain its small population. The simulated STM images based on this structure reproduce the filled-state STM image of the γ defect reasonably.

An extra discovery made in this study is the switching between the α and β species. The protrusion of the β structure in the STM image of Fig. 4(a) switches to the depression of α in the subsequent STM image of Fig. 4(b) (indicated by the arrow). This behavior is manifested in the STM image of Fig. 4(c); during the scanning on this particular defect, the central topographic feature switches back and forth between the protrusion and the depression [Fig. 4(c)]. The switching between these two defects is consistent with the proposed structure models for the α and β defects on the same adsorption site. However, the energy barrier between these two structures is calculated to be substantial, 0.5 eV, which is not easy to overcome thermally. We thus suggest that the

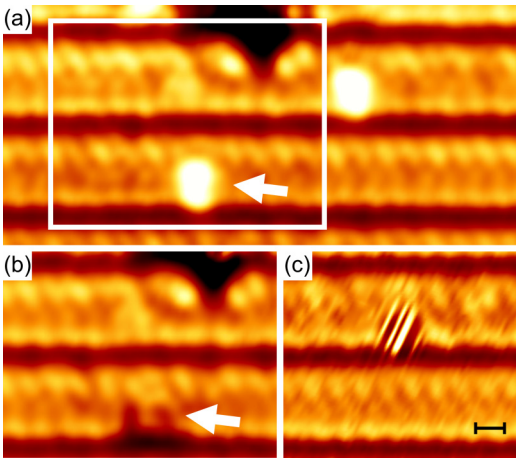

FIG. 4. (Color online) Sequential STM images showing the switching between an α (a) and a β (b) defect. (b) Refers to the area enclosed by the box in (a) after 14 min. (c) The STM image showing the fluctuation between the α and β defects during the scanning. All STM images were taken with $V_s = +0.4$ V and $I_t = 50$ pA. The scale bar represents 0.5 nm.

observed switching is assisted by the energy transfer through the tunneling current or the strong local electric field imposed by the tunneling bias.

Among the various atomic structure models reported for the adsorbates on the 4×1-In surface, there is no structure similar to α and β proposed in this study. For Pb, O, and In adatoms, only the interchain sites were considered [31]. As for a hydrogen adatom, the site between the In zigzag chain and the Si zigzag chain was suggested [30,31]. In case of Na, the sites between two In zigzag chains and those between the In and Si chains are energetically almost degenerate [20]. The unique atomic structure of the oxygen adsorbate could be important in understanding the T_c enhancement by oxygen.

On the other hand, the local lattice distortion around the oxygen adsorbate may play a role for the CDW phase transition, where the coupling with the lattice is crucial. We thus scrutinize the lattice structures around isolated oxygen adsorbates using the STM images. Indeed, the STM images, acquired at −0.4 V, reveal the occurrence of ×2 ($2a_0$ with $a_0 = 0.384$ nm, the Si lattice constant) distortions around adsorbates (Fig. 5). The distortions are clearly visible in the line profiles; the height of ×1 protrusions along In zigzag chains alternate as indicated by the dots. However, these distortions decay rapidly away from adsorbates; the decay length is (6∼7)a_0 along the wire. The modulation appears only along the In zigzag chain with the depression (protrusion) in the α (β) defect [Figs. 5(a) and 5(b)] as naturally expected from its intrachain adsorption structure. In contrast, the ×2 modulation is discovered on the In zigzag chain without the depression for the γ structure [Fig. 5(c)]. This difference can be explained by the atomic structure model of the γ defect [Fig. 3(d)], the interchain site with a shorter distance to one of the chains. The DFT calculations (Fig. 3) and the simulated STM images (Fig. 2) capture the essential features of those lattice distortions well. In particular, in the calculation for the

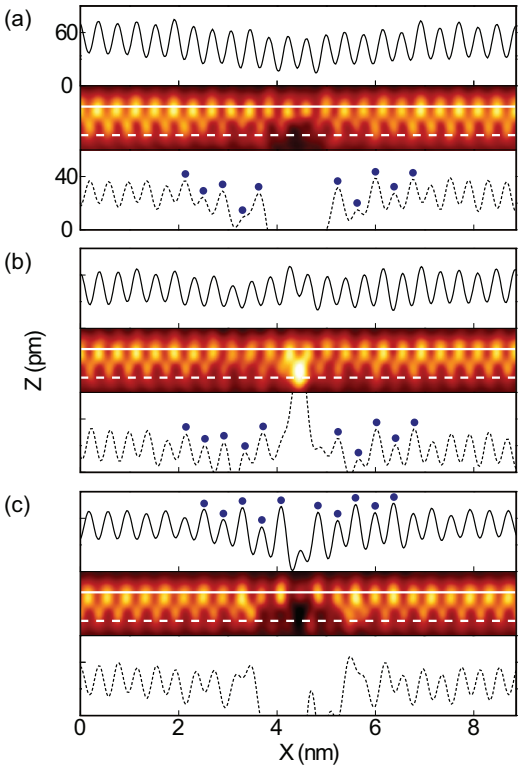

FIG. 5. (Color online) STM images ($V_s = -0.4$ V, $I_t = 50$ pA, 8.9 nm × 1.3 nm) with line profiles around (a) α, (b) β, and (c) γ defects (the z scale is the same in all images). For each image, two line profiles are taken along the two In zigzag chains (solid and dashed lines). The blue dots on the line profiles indicate the height modulations around the oxygen-induced defect.

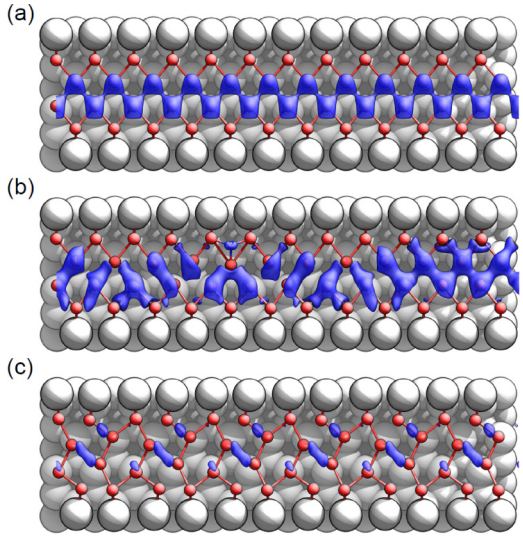

FIG. 6. (Color online) Local DOS plots for (a) the pristine In wire and (b) that with a single α oxygen adsorbate. The DOS within ±0.1 eV from the Fermi energy are integrated and the plots are made at isodensity of 0.001 Å^{-3}. While the total DOS within this energy range exhibits no noticeable change, the local DOS modification is consistent with the change of the STM image after the oxygen adsorption. (c) A similar plot for the pristine In wire in the 8×2 CDW state (at a much reduced isodensity of 0.0003 Å^{-3}). The DOS within ±0.1 eV are depleted due to the CDW gap formation.

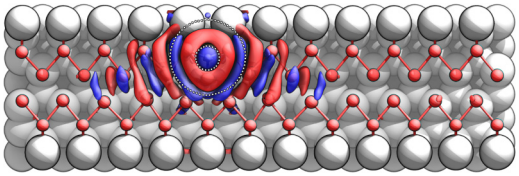

FIG. 7. (Color online) Change of the electron density after the adsorption of the oxygen in the α site; blue (red) for the accumulation (depletion) of the electron. The isodensity of the electron density plot is 0.001 $e^-/\text{Å}^{-3}$.

γ defect, only the In chain with a single In-O bonding is distorted significantly.

Note that the ×2 distortions around oxygen adsorbates are unambiguously distinguished from the 8×2 CDW structure. That is, STM images of the ×2 distortions around the oxygen adsorbates are apparently distinct from that of the 8×2 CDW phase below T_c with a large oval-shape protrusion centered between the two In chains [32]. We also find no band gap opening for the oxygen-induced distortions in our own scanning tunneling spectroscopy measurements. Our DFT calculation corroborates this; the total DOS near the Fermi level does not show any noticeable change upon the oxygen-induced distortions. However, the local DOS near the Fermi level follows ×2 distortions as shown in Fig. 6(b). This is in stark contrast to the 8×2 structure, which exhibits no substantial local DOS around the Fermi energy due to the gap opening. The present lattice distortions are instead similar to the ×2 distortions observed around hydrogen adsorbates [30]. Note that the CDW phase transition is suppressed on the hydrogen-adsorbed surface [17,19]. Therefore, we can reasonably suggest that the T_c enhancement of the oxygen-adsorbed surface is not directly related to the oxygen-induced structural distortions of In wires.

Beyond the distortion of the lattice, an oxygen adsorbate can transfer charge into the In wires. Figure 7 shows the lateral charge transfer induced by a single α defect. On the oxygen site (within the smaller dashed circle), the adsorbate attracts 0.42 electrons locally due to the partially ionic O-In bonding. However, beyond this bonding and the first-nearest neighbors (beyond the large dashed circle), the charge transfer is marginal with only 0.07 electrons transferred into this sphere in total. Given this amount of charge transfer, for low oxygen coverages, the doping effect to the In wires cannot be substantial as the recent ARPES study indicated [24]. Thus the doping mechanism for the T_c enhancement can be excluded safely. Considering all the information provided in the present study, we can suggest two possible scenarios of the T_c enhancement: (i) the lattice distortion induced by the adsorbate may lower the energy barrier into the 8×2 structure through the dynamical effect of relevant phonons and (ii) not a single adsorbate but multiple adsorbates may cooperate to induce the condensation of the 8×2 structure. These two scenarios need to be examined in the forthcoming studies.

IV. SUMMARY

The STM study and DFT calculations were carried out in order to investigate the oxygen adsorption on the Si(111)4×1-In surface, which leads to the T_c enhancement for the phase transition into an insulating CDW phase [17,19,24]. Our STM images reveal three distinct oxygen-induced defects on the 4×1-In surface denoted as α, β, and γ with characteristic bias dependencies. The α defect is the most commonly observed with a population of almost 70%. We found three energetically favorable adsorption structures by DFT calculations. The simulated STM images of these structures agree well with the bias-dependent STM images of oxygen-induced defects. The switching between the α and β defects observed in the STM images supports the atomic structure models, sitting on the same In intrachain site. The ×2 distortions around the oxygen adsorbates were characterized and the atomic structure models reproduce these distortions too. The distortions are distinguished from the 8×2 CDW phase but very similar to the ×2 distortion around hydrogen adsorbates [30], which is known to decrease the T_c of this surface. We thus suggest that the structural distortions of In wires due to the oxygen adsorption may not play the direct role for the T_c enhancement. The charge transfer of the adsorbate into the surface was shown to be marginal in agreement with the recent ARPES study. The present study also indicates that the oxygen adsorbates are mostly not mobile at room temperature ruling out the possible effect of the nonrandom distribution of adsorbates on the phase transition. While the present work excludes most of the possible mechanisms of the T_c enhancement proposed, we suggest two possible scenarios to be tested further: (i) the dynamical effect of the adsorbate in terms of phonons and (ii) the cooperative effect of multiple adsorbates. A further variable-temperature STM study is highly requested to address the origin of the T_c enhancement due to the oxygen adsorption. The atomic structures of the oxygen-induced defects established in this work would be a solid foundation for further studies on the intriguing T_c enhancement.

ACKNOWLEDGMENTS

This work was supported by Institute for Basic Science (IBS, Grant No. IBS-R014-D1). The numerical calculations were done using grants of computer time from Rechenzentrum Garching (RZG), the Paderborn Center for Parallel Computing (PC^2), and the Hochstleistungs-Rechenzentrum Stuttgart (HLRS). The Deutsche Forschungsgemeinschaft (DFG) is acknowledged for financial support (FOR1700).

[1] Z. Chen, J. Appenzeller, Y.-M. Lin, J. Sippel-Oakley, A. G. Rinzler, J. Tang, S. J. Wind, P. M. Solomon, and P. Avouris, Science **311**, 1735 (2006).

[2] W. Lu and C. M. Lieber, Nat. Mater. **6**, 841 (2007).

[3] M. Bockrath, D. H. Cobden, J. Lu, A. G. Rinzler, R. E. Smalley, L. Balents, and P. L. McEuen, Nature (London) **397**, 598 (1999).

[4] H. W. Yeom, S. Takeda, E. Rotenberg, I. Matsuda, K. Horikoshi, J. Schaefer, C. M. Lee, S. D. Kevan, T. Ohta, T. Nagao, and S. Hasegawa, Phys. Rev. Lett. **82**, 4898 (1999).

[5] H. Rauf, T. Pichler, M. Knupfer, J. Fink, and H. Kataura, Phys. Rev. Lett. **93**, 096805 (2004).

[6] W. H. Choi, P. G. Kang, K. D. Ryang, and H. W. Yeom, Phys. Rev. Lett. **100**, 126801 (2008).

[7] G. Grüner, *Density Waves in Solids* (Addison-Wesley Publishing Company, Reading, MA, Advanced Book Program, 1994).
[8] H. Fukuyama and P. A. Lee, Phys. Rev. B **17**, 535 (1978).
[9] P. A. Lee and T. M. Rice, Phys. Rev. B **19**, 3970 (1979).
[10] I. Bâldea and M. Bădescu, Phys. Rev. B **48**, 8619 (1993).
[11] X.-L. Wu, P. Zhou, and C. M. Lieber, Phys. Rev. Lett. **61**, 2604 (1988).
[12] H. Dai, H. Chen, and C. M. Lieber, Phys. Rev. Lett. **66**, 3183 (1991).
[13] H. Dai and C. M. Lieber, Phys. Rev. Lett. **69**, 1576 (1992).
[14] H. Bando, K. Koizumi, Y. Miyahara, and H. Ozaki, J. Phys.: Condens. Matter **12**, 4353 (2000).
[15] J.-H. Cho, D.-H. Oh, K. S. Kim, and L. Kleinman, Phys. Rev. B **64**, 235302 (2001).
[16] S. V. Ryjkov, T. Nagao, V. G. Lifshits, and S. Hasegawa, Surf. Sci. **488**, 15 (2001).
[17] G. Lee, S.-Y. Yu, H. Shim, W. Lee, and J.-Y. Koo, Phys. Rev. B **80**, 075411 (2009).
[18] H. Morikawa, C. C. Hwang, and H. W. Yeom, Phys. Rev. B **81**, 075401 (2010).
[19] T. Shibasaki, N. Nagamura, T. Hirahara, H. Okino, S. Yamazaki, W. Lee, H. Shim, R. Hobara, I. Matsuda, G. Lee, and S. Hasegawa, Phys. Rev. B **81**, 035314 (2010).
[20] W. G. Schmidt, M. Babilon, C. Thierfelder, S. Sanna, and S. Wippermann, Phys. Rev. B **84**, 115416 (2011).
[21] S. Wall, B. Krenzer, S. Wippermann, S. Sanna, F. Klasing, A. Hanisch-Blicharski, M. Kammler, W. G. Schmidt, and M. Horn-von Hoegen, Phys. Rev. Lett. **109**, 186101 (2012).
[22] H. Shim, J. Yeo, G. Lee, and H. Kim, Phys. Rev. Lett. **111**, 149601 (2013).
[23] T. Frigge, S. Wall, B. Krenzer, S. Wippermann, S. Sanna, F. Klasing, A. Hanisch-Blicharski, M. Kammler, W. G. Schmidt, and M. Horn-von Hoegen, Phys. Rev. Lett. **111**, 149602 (2013).
[24] S. H. Uhm and H. W. Yeom, Phys. Rev. B **88**, 165419 (2013).
[25] A. B. Harris, J. Phys. C: Solid State Phys. **7**, 1671 (1974).
[26] Y. Imry and M. Wortis, Phys. Rev. B **19**, 3580 (1979).
[27] M. Aizenman and J. Wehr, Phys. Rev. Lett. **62**, 2503 (1989).
[28] D. M. Ceperley and B. J. Alder, Phys. Rev. Lett. **45**, 566 (1980).
[29] G. Kresse and J. Furthmüller, Comput. Mater. Sci. **6**, 15 (1996).
[30] G. Lee, S.-Y. Yu, H. Kim, and J.-Y. Koo, Phys. Rev. B **70**, 121304 (2004).
[31] S. Wippermann, N. Koch, and W. G. Schmidt, Phys. Rev. Lett. **100**, 106802 (2008).
[32] T.-H. Kim and H. W. Yeom, Phys. Rev. Lett. **109**, 246802 (2012).